

Viewing Zone Evaluation and Analyses of the Holographic Images Reconstructed by 1- μm Ferroelectric Liquid Crystal Pixel Arrays

Shintaro Aso¹, Kisho Yamamoto², Ken-ichi Aoshima¹, Junichi Shibasaki¹, Ryo Higashida¹, Nobuhiko Funabashi¹, Takahiro Ishinabe², Yosei Shibata², Hideo Fujikake², Kenji Machida¹

asou.s-iy@nhk.or.jp

¹NHK, 1-10-11 Kinuta, Setagaya-ku, Tokyo 157-8510, Japan

²Tohoku University, 6-6-05 Aoba, Aramaki, Aoba-Ku, Sendai, Miyagi 980-8579, Japan

Keywords: Holographic Display, Spatial Light Modulator, Ferroelectric Liquid Crystal

ABSTRACT

We found the brightness of holographic images reconstructed by a ferroelectric liquid crystal (FLC) pixel array depend on observation-angles, and clarified the dependence is attributed to the diminished diffracted light which is caused by passing through the adjacent pixel with different FLC alignment.

1 Introduction

Holography [1] is a technology that displays three-dimensional (3D) objects by recording and reconstructing the light wavefront emitted by the object. Although it is considered as the ultimate 3D imaging method, realizing a practical viewing-zone angle of a reconstructed holographic image requires a spatial light modulator (SLM) with a pixel pitch as small as the visible wavelength. In order to accomplish this, a liquid crystal (LC) SLM with a pixel pitch of $1 \times 9 \mu\text{m}$ was recently reported [2]. To reduce the pixel pitch of the LC-SLM further, we demonstrated the individual pixel driving of ferroelectric liquid crystal (FLC) pixels with a pixel pitch of $1 \times 1 \mu\text{m}$ by displaying a checkered pattern using a uniquely developed predesigned two-layered electrode [3]. Furthermore, we demonstrated a 3D holographic image reconstruction with a viewing-zone angle of over 30° using a $10\text{k} \times 10\text{k}$ FLC pixel array with a pixel pitch of $1 \times 1 \mu\text{m}$ [3]. However, at higher diffraction angles, the reconstructed holographic images darkened, implying that diffracted light was affected by closely arranged adjacent pixels. We investigated the viewing angle characteristics of reconstructed holographic images using FLC when the incident angle and polarization state of the reference beam was changed in this study. In addition, to investigate the mechanism of the viewing angle characteristics of the reconstructed holographic images, we approximated the FLC pixel array as very simplified two-dimensional models of FLC diffraction gratings with different binary switching angles of FLC between adjacent pixels and calculated the diffraction efficiencies by using rigorous coupled-wave analysis (RCWA).

2 Experiment

2.1 Structure of the FLC Pixel Arrays Displaying a Computer-generated Hologram (CGH) with a Pixel Pitch of $1 \times 1 \mu\text{m}$

Fig. 1 shows the schematic illustration of the structures of the fabricated FLC pixel arrays, which display a static binary CGH with a pixel pitch of $1 \times 1 \mu\text{m}$. In this study, we made both reflective and transmissive pixel arrays. The reflective array has a two-layered electrode consisting of a lower-layer electrode of ruthenium (Ru) (20 nm), a SiO_2 insulation layer (320 nm), and an upper-layer electrode of indium-zinc-oxide (IZO) (20 nm) on a silicon substrate. The upper-layer electrode has square apertures arranged to form a CGH pattern, which comprises $10\text{k} \times 10\text{k}$ pixels and a pixel pitch of $1 \times 1 \mu\text{m}$. The each aperture was $0.8 \times 0.8 \mu\text{m}$ in size. To achieve an anti-parallel LC alignment along the y-axis, alignment films (AL-1254; JSR Co.) were spin-coated on the two-layered and counter transparent common electrodes, and a rubbing treatment was applied. An FLC mixture was sealed between the two-layered and the common electrode with a layer thickness of $1 \mu\text{m}$. The transmissive array also has the same design as the FLC layer of the reflective array, while that has a two-layered electrode, comprising transparent lower- and upper-layer electrodes of IZO (20 nm) and SiO_2 insulation layer (160 nm) on a transparent glass substrate. The aperture dimension of the upper-layer electrode in the transmissive array was $0.9 \times 0.9 \mu\text{m}$. To estimate the electric potential distribution at the interface between the two-layered electrode and FLC layer, a finite element calculation was carried out [3]. In the case of the calculation for the transmissive pixel array, we applied +4.8 V to the lower-layer electrode and -2.2 V to the upper-layer electrode of the two-layered electrode, and the common electrode was maintained at 0 V. The relative permittivity of the FLC insulating layers were 2.8 and 4.3, respectively. The calculated electric potential at the interface between the two-layered electrode and FLC layer was -2.2 V in the upper-layer electrode and

around +1.0 V in the aperture of the upper-layer electrode. Thus, the positive and negative voltage distribution on the two-layered electrode drives FLC pixel array, which displays a CGH corresponding to the aperture pattern in the upper-layer electrode.

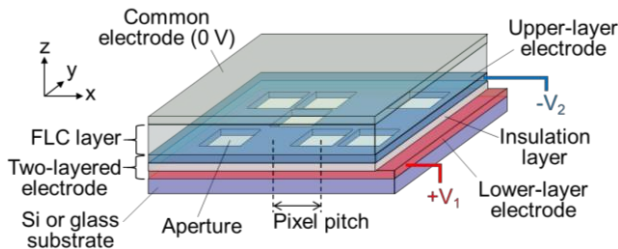


Fig. 1 Schematic illustration of a perspective view of fabricated FLC pixel arrays

2.2 Reconstruction of a Hologram

Fig.2 shows a top view of the optical setup of the reconstruction of the hologram using the reflective or transmissive FLC pixel arrays. In the case of using the reflective pixel array, a He-Ne laser beam (wavelength of 632.8 nm) was expanded by a beam expander and introduced into the pixel array at an incident angle of 20° through a polarizer with polarization directions of $+22.5^\circ$ or $+112.5^\circ$ clockwise from the y-axis when viewed from the light source. Modulated light in the pixel array was observed from various angles by a CMOS image sensor with an analyzer that was orthogonal to the polarization direction of the incident light. The pixel array was placed at an angle of $+9^\circ$ from the y-axis to the z-axis and the CMOS image sensor was placed at an elevation angle of 6° to prevent the zero-order diffraction light from entering the CMOS image sensor. (These tilt angles are not shown in Fig. 2.) θ is the observation angle of the reconstructed holographic images. In the case of using the transmissive pixel array, a beam expander expanded a He-Ne laser beam and introduced it perpendicular to the pixel array via a polarizer with a polarization direction of $+112.5^\circ$ from the y-axis to the x-axis. A CMOS image sensor with an analyzer orthogonal to the polarization direction of the incident light observed modulated light in the pixel array from various angles. The CMOS image sensor was placed at a depression angle of 8° to prevent the zero-order diffraction light from entering the CMOS image sensor.

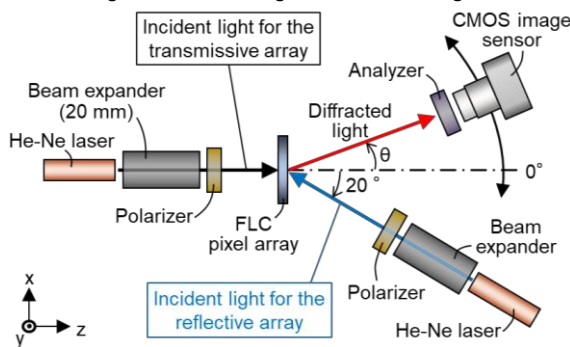


Fig. 2 Top view of the Optical setup of the

reconstruction of the hologram

3 Results and Discussion

3.1 Polarizing Micrograph

Fig. 3 shows a polarizing micrograph of a fabricated reflective FLC pixel array. The direction of the polarizer was $+22.5^\circ$ clockwise from the y-axis, and the analyzer was orthogonal to the polarizer. The LC alignment direction was parallel to the y-axis. We applied +4.8 V to the lower-layer electrode, -2.2 V to the upper-layer electrode of the two-layered electrode, and 0 V to the common electrode. Clear black and white pixels can be seen, indicating a successful display of an interference fringe pattern of the designed CGH with a pixel pitch of $1 \times 1 \mu\text{m}$.

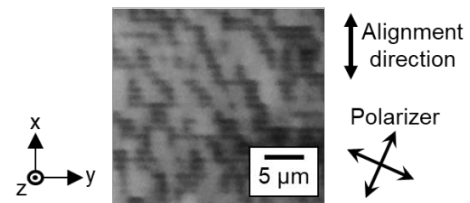


Fig. 3 Polarizing micrograph of the fabricated reflective FLC pixel array

3.2 Reconstruction of a Hologram

Fig. 4 shows the reconstructed holographic images of the fabricated reflective FLC pixel array observed by the optical setup shown in Fig. 2. When the incident light was viewed from the light source, the polarization direction was $+22.5^\circ$ clockwise from the y-axis. The center of the viewing-zone angle was $+20^\circ$ because the incident light was introduced into the array at a 20° incident angle. The expected viewing-zone angle of the reconstructed holographic image was over 36° (i.e., the holographic image was expected to be observed in θ from $+2^\circ$ to $+38^\circ$ in Fig. 2) at a light source wavelength of 632.8 nm because the pixel pitch of the designed CGH was $1 \times 1 \mu\text{m}$. However, the holographic image observed at $+38^\circ$ was darker than the image at $+2^\circ$. Furthermore, we observed holographic images reconstructed from the same reflective FLC pixel array using the incident light with another polarization direction of $+112.5^\circ$ clockwise from the y-axis when viewed from the light source with the same optical setup shown in Fig. 2. In this case, the holographic image observed at $+2^\circ$ was darker than the image at $+38^\circ$. Thus, observed holographic images reconstructed by the incident light with the different polarization directions got dark at the different observation angles and both images varied in brightness depending on the observation angle. Fig. 5 shows the reconstructed holographic images of the fabricated transmissive FLC pixel array observed by the optical setup shown in Fig. 2. The polarization direction of the incident light was $+112.5^\circ$ from the y-axis to the x-axis. Though the holographic images observed

at -18° and $+18^\circ$ were slightly darker than the image observed at 0° , the brightness of the images observed at -18° and $+18^\circ$ were nearly identical.

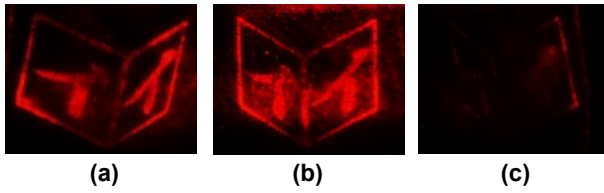


Fig. 4 Holographic images of the reflective FLC pixel array reconstructed by the incident light with the polarization direction of $+22.5^\circ$ clockwise from the y-axis, observed from (a) $+2^\circ$, (b) $+20^\circ$, and (c) $+38^\circ$

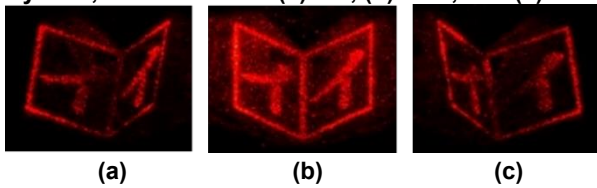


Fig. 5 Reconstructed holographic images of the transmissive FLC pixel array observed from (a) -18° , (b) 0° , and (c) $+18^\circ$

3.3 Diffraction Calculation of FLC Gratings Using a Simple Two-dimensional Binary Light Modulator Model

The brightness of the holographic images reconstructed with a 20° incident angle showed a large dependence on the observation angles, as described in section 3.2, and the dependence varied with the polarization directions of the incident light. In order to investigate this mechanism, the fabricated FLC pixel arrays were approximated to simplified two-dimensional models of FLC diffraction gratings shown in Figs. 6 (a) and (b) those have different binary switching angles of FLC between adjacent pixels (i.e., areas A and B in the figures) and the diffraction efficiencies were calculated by using the RCWA method. Holographic images are made up of first-order diffracted light from interference fringes with different fringe pitches. Calculating the -1 st and $+1$ st order diffraction efficiencies of the FLC gratings with a pixel pitch of $1\ \mu\text{m}$, as shown in Figs. 6 (a) and (b), allows us to estimate the -1 st and $+1$ st order diffraction efficiencies of the diffracted light produced by the smallest fringe pitch of $1\ \mu\text{m}$ displayed by the fabricated FLC pixel arrays. In theory, this influences the brightness of the reconstructed holographic images at the outermost viewing-zone angle (i.e., holographic images observed at the largest diffraction angle). The reflective and transmissive calculation models are shown in Figs. 6 (a) and (b), respectively. FLC with the binary alignment directions shown in Fig. 7 was placed in areas A and B. In this calculation, it is assumed that the FLC is approximated to a uniaxial anisotropic medium with an extraordinary ray refractive index $n_e = 1.663$ and an ordinary ray refractive index $n_o = 1.5$, and that all the FLC molecules are aligned at angles shown in Fig. 7 with

respect to the layer thickness direction (i.e., the z-axis direction). Since the FLC mode was the surface stabilized ferroelectric liquid crystal mode in this experiment, the switching directions were binary angles of $\pm 22.5^\circ$ as shown in Fig. 7, depending on the applied electric field. Correspondingly, the polarization directions of the incident light were set to two different conditions of $+22.5^\circ$ and $+112.5^\circ$ from the y-axis to the x-axis. The incident light had a wavelength of $632.8\ \text{nm}$. In Fig. 6 (a), the refractive index and extinction coefficient of aluminum were 1.4 and 7.6, respectively. Air had a refractive index of 1.0. No analyzer was used to observe the diffracted light for the sake of calculation, and the diffraction efficiencies with complex amplitude modulation were calculated. θ_{-1} and θ_{+1} in Figs. 6 (a) and (b) are -1 st and $+1$ st order diffraction angles, respectively. Fig. 8 shows the -1 st, 0 th, and $+1$ st order diffraction efficiencies calculated by the models shown in Figs. 6 (a) and (b). In Fig. 8, red square dots (a) show diffraction efficiencies calculated by the model shown in Fig. 6 (a) with the incident light with the polarization direction of $+22.5^\circ$ from the y-axis to the x-axis. The -1 st and $+1$ st order diffraction efficiencies were 0.15 and 0.09, respectively. Thus, the diffraction efficiency of the $+1$ st order diffracted light which appeared on the larger angle was smaller. This result is considered to correspond to the dark holographic image of Fig. 4 (c), which was observed at the largest observation angle. On the other hand, blue triangle dots (b) in Fig. 8 show diffraction efficiencies calculated by the model shown in Fig. 6 (a) with the incident light with the polarization direction of $+112.5^\circ$ from the y-axis to the x-axis. The -1 st and $+1$ st order diffraction efficiencies were 0.12 and 0.25, respectively. Thus, the diffraction efficiency of the -1 st order diffracted light which appeared on the smaller angle was smaller. These calculated results are considered to correspond to the results as described in section 3.2 (i.e., the observed holographic images reconstructed by the incident light with the different polarization directions got dark at the different observation angles and both images varied in brightness depending on the observation angle.) Finally, black circle dots (c) in Fig. 8 show the -1 st, 0 th, and $+1$ st order diffraction efficiencies calculated by the model shown in Fig. 6 (b) with the incident light with a polarization direction of $+112.5^\circ$. The -1 st and $+1$ st order diffraction efficiencies were the same value of 0.12. This result is considered to correspond to the almost same brightness of the observed holographic images shown in Figs. 5 (a) and (c). Thus, although Figs. 6 (a) and (b) were very simplified models, the calculation results of the -1 st and $+1$ st order diffraction efficiencies corresponded to the observed change in the brightness of the reconstructed holographic images due to the observation angle in Figs. 4 and 5. This indicates that the observed change in the

brightness of the reconstructed holographic images due to the observation angle in Figs. 4 and 5 can be explained by the models shown in Figs. 6 (a) and (b). According to the Fig. 8, the +1st order diffraction angle calculated by the model shown in Fig. 6 (a) was $+41.2^\circ$. From this, it is considered that most of the +1st-order diffracted light, which was modulated while propagating in the $1\ \mu\text{m}$ thick FLC layer, passed through both the areas A and B in Fig. 6 (a) because the width of the areas A and B is extremely small and the same as the FLC layer thickness. On the other hand, since the -1st order diffraction angle was $+1.5^\circ$, it is considered that most of the -1st-order diffracted light passed only through either area A or B in Fig. 6 (a). In this way, since the refractive index distributions in the propagation paths of the -1st and +1st order diffracted light was significantly different from each other, a large difference also occurred in the diffraction

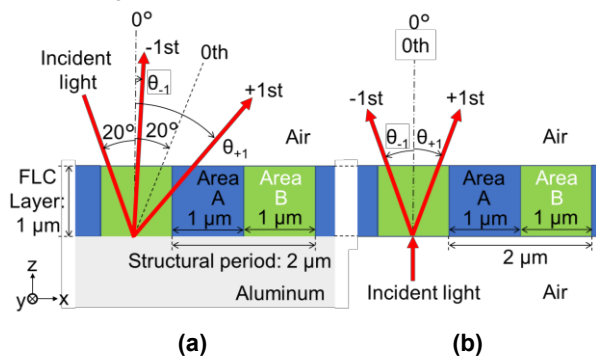


Fig. 6 Calculation models of the diffraction efficiencies of (a) a reflective and (b) a transmissive FLC diffraction gratings

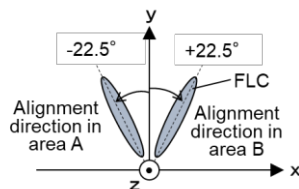


Fig. 7 Definition of alignment directions of FLC in the calculation models shown in Figs. 11 and 12

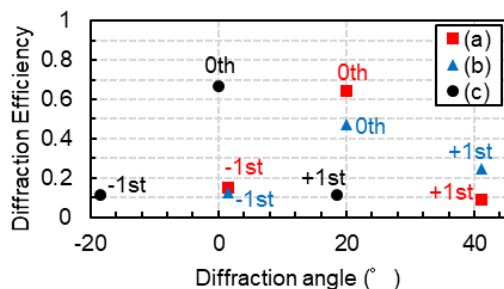


Fig. 8 Calculation results of the diffraction efficiencies of FLC diffraction gratings. (a) and (b) show the results for the reflective grating with the incident light with the polarization directions of (a) $+22.5^\circ$ and (b) $+112.5^\circ$ from the y-axis to the x-axis. (c) shows the result for the transmissive grating.

efficiencies, which is considered to have led to a large difference in the brightness of the observed holographic image depending on the observation angle in Fig. 4. Whereas, according to Fig. 8, the -1st and +1st order diffraction angles calculated by the model shown in Fig. 6 (b) were -18.4° and $+18.4^\circ$, respectively, and had the same absolute value. Thus, the refractive index distributions in the propagation paths of the -1st and +1st order diffracted light was almost symmetrical for each pixel, which is considered to have led to the almost same brightness of the reconstructed holographic images observed at -18° and $+18^\circ$ shown in Fig. 5.

4 Conclusions

When the reference beam (i.e., the incident light) is incident obliquely on a holographic display using FLC with a pixel pitch of the thickness of the FLC layer, the leakage of the diffracted light to the adjacent pixels increases and the viewing angle characteristic deteriorates. Thus, the reference beam should be incident perpendicularly on a holographic display using FLC with an extremely small pixel pitch and a wide viewing-zone angle. The influence of light leakage to adjacent pixels increases as the diffraction angle increases as the pixel pitch decreases. Furthermore, we discovered that the influence on the viewing angle characteristics of holographic displays using FLC when changing the incident angle and polarization state of the reference beam can be estimated to some extent by using a very simple diffraction efficiency calculation model, as shown in Figs. 6 (a) and (b). This result proposes a new design method for LC holographic displays with a wide-viewing zone angle.

Acknowledgments

We would like to thank Dr. Yoshitomo ISOMAE, a former student of Tohoku University, for fabricating the FLC layer of the reflective FLC pixel array.

References

- [1] E. N. Leith and J. Upatnieks, "Reconstructed wavefronts and communication theory," *J. Opt. Soc. Am.*, Vol. 52, No. 10, pp. 1123–1130 (1962).
- [2] C. S. Hwang, J. H. Choi, J. E. Pi, J. H. Yang, G. H. Kim, Y. H. Kim, J. Y. Kim, W. J. Lee, H. O. Kim, H. K. Lee, M. Y. Kim and J. Kim, "1 μm pixel pitch spatial light modulator panel for digital holography," *SID 2020 Digest*, pp. 297–300 (2020).
- [3] S. Aso, Y. Isomae, K. Aoshima, R. Higashida, N. Funabashi, J. Shibasaki, T. Ishinabe, Y. Shibata, K. Machida, H. Fujikake and H. Kikuchi, "A two-dimensionally aligned array with 1- μm pixel pitch using ferroelectric liquid crystal pixels for holography application," *SID 2020 Digest*, pp. 17–20 (2020).